SPATIO-TEMPORAL AND CROSS-SCALE INTERACTIONS IN HYDROCLIMATE VARIABILITY: A CASE-STUDY IN FRANCE

Manuel Fossa[1], Bastien Dieppois[2], Nicolas Massei[1], Matthieu Fournier[1], Benoit Laignel[1], and Jean-Philippe Vidal[3]

[1]   Normandie Univ, UNIROUEN, UNICAEN, CNRS, M2C, 76000 Rouen, France
[2]   Centre for Agroecology, Water and Resilience (CAWR), Coventry University, Coventry, UK
[3]   INRAE, UR Riverly, 5 rue de la Doua, CS 20244, 69625 Villeurbanne Cedex, France

Correspondence: Manuel Fossa (manuel.fossa1@univ-rouen.fr)

Abstract. Understanding how water resources vary at different temporal and spatial scales in response to climate is crucial to inform long-term management. Climate change impacts and induced trends may indeed be substantially modulated by low-frequency (multi-year) variations, whose strength varies in time and space, with large consequences on risk forecasting systems. In this study, we present a spatial classification of precipitation, temperature and discharge variability in France, based on a fuzzy clustering and wavelet spectra of 152 near natural watersheds between 1958 and 2008. We also explore phase-phase and phase-amplitude causal interactions between time scales of each homogeneous region. Three significant time scales of variability are found in precipitation, temperature and discharge: 1 year, 2-4 years and 5-8 years. The magnitude of those time scales of variability is however not constant over the different regions. For instance, Southern regions are markedly different from other regions, with much lower 5-8 years variability and much larger 2-4 years variability. Several temporal changes in precipitation, temperature and discharge variability are identified during the 1980s and 1990s. Notably, we note a sudden decrease in annual temperature variability in the mid 1990s in the Southern half of France. Investigating cross-scale interactions, our study reveals causal and bi-directional relationships between higher and lower-frequency variability, which may feature interactions within the coupled land-ocean-atmosphere systems. Interestingly, however, even though time-frequency patterns (occurrence and timing of time scales of variability) were similar between regions, cross-scale interactions are far much complex, differ between regions, and are not systematically transferred from climate variability (precipitation and temperature) to hydrological variability (discharge). Phase-amplitude interactions are indeed absent in discharge variability, although significant phase-amplitude interactions are found in precipitation and temperature. This suggests that watershed characteristics cancel the negative feedback systems found in precipitation and temperature.This study allows for a multi-time scale representation of hydro-climate variability in France, and provides unique insight into the complex non-linear dynamics of this variability, and its predictability.

1   Introduction

Hydroclimate variability represents the spatio-temporal evolution of hydrological variables (e.g. discharge, groundwater level) and climate variables (e.g. precipitation and temperature), which are directly impacting hydrological variability. Studying how

hydrological variables react to climate variability and change is a major challenge for society, in particular for water resource

25 management, flood and drought mitigation planning (IPCC, 2007, 2014). However, hydrological variability is expressed at multiple time scales (Labat, 2006; Schaefli et al., 2007; Massei et al., 2007, 2017), for which driving mechanisms remains poorly characterised and understood. As suggested in Blöschl et al. (2019), understanding the spatio-temporal scaling, i.e. how the general dynamics driving hydrological variability change at spatial and temporal scales, represents a major challenge toward improved prediction systems (Gentine et al., 2012). Understanding spatio-temporal scaling required to identify regions,

30 i.e. the maximum spatial scale in which the dynamics remain unchanged despite its non-linearity, is critical (Hubert, 2001). Hydrological variability is by definition non-linear (Labat, 2000; Lavers et al., 2010; McGregor, 2017), as it results from complex interactions between atmospheric dynamics and catchment properties that may vary at different time scales (e.g. soil characteristics, water table, karstic systems, vegetation covers;(Gudmundsson et al., 2011; Sidibe et al., 2019)). Such interactions between processes at different time scales, i.e. cross-scale interactions (Paluš, 2014; Jajcay et al., 2018), have

35 however never been studied to further understand hydrological variability, as well as its link to climate. It has also been shown that hydroclimate variability is inherently non-stationary, with sudden changes in the dynamics of the system, due to a change in the balance between its driving physical processes (e.g. Coulibaly and Burn (2004); Labat (2006); Dieppois et al. (2013, 2016); Massei et al. (2017)).This results in difficulties in characterizing and predicting the hydrological variability at different spatio-temporal scales (Gentine et al., 2012; Blöschl et al., 2019).

40 While different time scales have been identified in hydrological variability at both regional and global scales (Coulibaly and Burn, 2004; Labat, 2006; Dieppois et al., 2013, 2016; Massei et al., 2017), very little has been done to explore how spatially coherent are those time scales, and therefore to identify regions in which the statistical characteristics of all ranges of variability remain unchanged. Studying 231 stream gauges throughout the world, Labat (2006) highlighted different time scales of discharge variability over the different continents. At the regional scale, Smith et al. (1998) established a clustering

45 of 91 US stream gauges based on their global wavelet spectra, i.e. dominant time scales, and found five homogeneous regions. Similarly,Anctil and Coulibaly (2004) and Coulibaly and Burn (2004) established a clustering of Southern Québec and Canada streamflow, based on the timing of both the 2-3 and 3-6 year time scales. In Europe, Gudmundsson et al. (2011) identified different regions according to the magnitude of decadal discharge variability. In France, such a clustering, based on time-frequency patterns of discharge variability, as well as its relation to climate variability (e.g. precipitation and temperature), has

50 not yet been explored. In addition, all studies mentioned above either isolated particular time scales or averaged the variability across time scales (e.g. global wavelet spectra), which is equivalent to a linearization of the system (Hubert et al., 1989). While studying cross-scale interactions have retained increasing interest in other fields (*e.g.* Onslow et al. (2014); Wang et al. (2014)), cross-scale interactions are poorly understood in climate and hydrological sciences. New strategies have recently been developed to facilitate such studies (Jajcay et al., 2018). Cross scale interactions are however very relevant to hydroclimate

55 studies, in particular when searching for climate drivers (or predictors) of hydrological signals, as they will reveal climate time scales causally linked to each time scale of hydrological variability.

In this study, we investigate the spatial homogeneity of hydroclimate variability across time scales. For instance, can we identify homogeneous regions according to particular time-scales? From the determination of homogeneous regions of hydro-

climate variability, we will explore and discuss possible interactions between hydroclimate processes and catchment properties,
60   that may partially explain each region's spectral content, through the study of their cross-scale interactions.

This study therefore have major implication for the comprehension of hydroclimate dynamics and their interactions with large-scale climate drivers, and catchment properties. The results of this study will provide guidance for operational uses, such as seasonal to multi-year forecasting, as they highlight the time scales that need to be focused on when improving models.

The work is divided into the following sections. Data and methods are introduced in Section 2. In Section 3, we establish
65   homogeneous regions for precipitation, temperature and discharge variability based on their time-frequency patterns and then explore cross-scale interactions for each region of homogeneous variability in precipitation, temperature and discharge. Finally, discussions of the main results and conclusions are provided in Section 4.

2   Data and methodology

2.1   Hydrological and climate data

70   Discharge time series were extracted from French Reference Hydrometric Newtork compiled by Giuntoli et al. (2013). This network of stations identifies near-natural watersheds with long-term high-quality hydrometric data. The period 1968-2008 was chosen by Giuntoli et al. (2013) as being the best trade-off in terms of data availability over the different regions. This database was further subset to 152 watersheds by selecting only continuous monthly time series, i.e. without missing values (Figure 1). Precipitation and temperature data have been estimated from the 8 km-grid Safran surface reanalysis dataset (Vidal
75   et al., 2010), which has been subset to a common period (1968-2008). For this study, precipitation and temperature have been averaged over each watershed area (Caillouet et al., 2017).

2.2   Methods

Figure 2 summarizes the different methods employed in this study.

2.2.1   Continuous wavelet transforms

80   Time-frequency patterns have first been extracted for each watershed and each variable using continuous wavelet transform (cf. Figure 2, (a)). For any finite energy signal x, it is possible to obtain a time-frequency representation by mapping it to a series of sub-spaces spawned by a generating function, the mother wavelet, and its scaled versions (Torrence and Compo, 1998; Grinsted et al., 2004). The time series is then represented in terms of a given scale and time location. The first subspace is generated by a mother wavelet at scale 1 and its time translations. Then, other subspaces are generated by scaling the mother wavelet
85   up, referring to daughter wavelets, and time translating it. For each scale, one subspace is constructed. Daughter wavelets are usually calculated as:

$$\psi_{a,b} = \frac{1}{\sqrt{a}} \psi(\frac{t-b}{a}) \tag{1}$$

The left hand side (LHS) term is the daughter wavelet of scale a and time translation b at time t. The first right hand side (RHS) term is the scaling of the mother wavelet ψ and the last one is the time translation. The projection of the signal onto each scale a is of the form:

$$WT_\psi[x](a,b) = \langle x, \psi_{a,b} \rangle = \int_R x(t)\psi_{a,b}(t)dt \qquad (2)$$

LHS term contains the wavelet coefficients, i.e. the coordinates of the signal in each subspace. If the mother wavelet (and hence the daughter wavelets as well) is complex, wavelet coefficients are complex as well. Wavelet coefficients represent the inner product of the signal and daughter wavelet of scale a and time translation b (Centre). The norm of their square is called the wavelet power and represents the amplitude of the oscillation of signal x at scale a and centred on time t. As it is impossible to capture the best resolution in both frequency and time simultaneously, we used here a Morlet mother wavelet (order 6), which offers a good trade-off between detection of scales and localisation of the oscillations in time (Torrence and Compo 1998). Statistical significance is typically tested against a red noise using Monte Carlo simulations (Torrence and Compo 1998).

2.2.2 Image Euclidean Distance Clustering

We estimated similarities between wavelet spectra of each watersheds and, separately, on each variable. Distances between two-dimensional data, such as maps or wavelet spectra, are estimated using Euclidean distance between pairwise points (pED; i.e computing $f_2(x_i, y_i) - f_1(x_i, y_i)$). However, such a procedure has no neighborhood notion, making it impossible to account for globally similar shapes (cf. definition of global and local similarity in Wang et al. (2005)). To avoid this issue, we used the Image Euclidean distance calculation method (hereinafter IEDC) developed by Wang et al. (2005). The IEDC method modifies the pED equation in two ways (Wang et al., 2005): i) the distance between pixel values is computed not only pairwise, but for all indices; ii) a Gaussian filter, function of the spatial distance between pixels, is applied. The Gaussian filter then applies less weight to the computed distance between very close and far apart pixels, while emphasizing on medium spaced ones (**?**).

2.2.3 Fuzzy clustering

Fuzzy clustering has then been used to cluster the different watershed based on their similarities (Figure 2, (b)). Fuzzy clustering is a soft clustering method (Dunn, 1973). While soft clustering spreads membership over all clusters with varying probability, hard clustering attributes each station one and only one cluster membership. Soft clustering is therefore better-suited when the spatial variability, originating from different stations' characteristics, is smooth, such as in hydroclimate data. For instance, precipitation and temperature patterns are unlikely to change suddenly from one station to a neighboring one, and in turn, be markedly different from the next neighbor (Moron et al., 2007; Hannaford et al., 2009; Rahiz and New, 2012). As such, several stations tend to show transitional or hybrid patterns, and can potentially be member of different clusters, limiting the robustness of hard clustering procedure (Liu and Graham, 2018).

Fuzzy clustering performance is determined by the ability of the algorithms to recognize hybrid stations (i.e. stations incorporating multiple features from different patterns observed in other coherent regions), while allowing for a clear determination

of the membership of stations with unique features (Kaufman and Rousseeuw, 1990). Here, we used the FANNY algorithm

120 (Kaufman and Rousseeuw, 1990), which has been shown to be flexible, and to offer the possibility to adapt the clustering to the data, with optimal performance (Liu and Graham, 2018). In addition, rather than setting the number arbitrarily, in this study, we used an estimation of the optimum number of clusters by first computing a hard clustering method: the consensus clustering (Monti et al., 2003). Thus, the number of clusters providing the best stability (i.e. the minimal changes of member-ship when adding new individuals) is considered optimal as recommended in Şenbabaoğlu et al. (2014). The different clusters'

125 memberships are then mapped to discuss the spatial coherence of each hydroclimate variable.

2.2.4 cross-scale interactions

For each variable and each cluster, cross-scale interactions have also been explored for the first time in hydrological sciences (Figure 2, (c)). Cross-scale interactions refer to phase-phase and phase-amplitude couplings between time scales of a given time series (Scheffer-Teixeira and Tort, 2016; Paluš, 2014). Here, coupling means that the state (either phase or amplitude) of a

130 signal y is dependent on the state of a signal x, and describes causal relationship (Granger, 1969; Pikovsky et al., 2001), which refers to information transfer from one part of a signal to another.

Figure 3 describes the necessary setting and characteristics of cross-scale interactions. A variable $f(t)$ measures the dy-namics of a physical process. This process is modelled as a coupling of two components X, and Y. The components interact with each other in a perturbation-dampening (X, Y, respectively), so that $f(t) = X - Y$ (Figure 3a). The interactions between

135 the components occur through the connections C_{XY} and C_{YX}, with a given strength (here $C_{..} = 2$), and this perturbation-dampening interaction forms a negative feedback system (Figure 3a). The connection C_{XX} enables X to grow first before Y dampens it, and both X and Y receive inputs ϕ_X, ϕ_Y from other physical processes (figure 3a). Depending on both the mean and time scales of ϕ_X and ϕ_Y, the strength of C_{XX}, C_{XY} and C_{YX}, X and Y may show coupled behaviors. For instance, in Figure 3b, every fourth ridges of $Y_{PP}(t)$ is synchronized with a ridge of $X(t)$ (Figure 3b, top and middle panels), thus forming

140 a phase-phase interaction. The direction of the interactions depends on the inputs ϕ_X, ϕ_Y, and the connections C_{XX}, C_{XY} and C_{YX}. $f_{PP}(t)$ is the difference between $X(t)$ and Y_{PP} (Figure 3b, bottom panel). Because the interaction between X and Y depends on both inputs and connections, interactions may lead to a cross-scale relationship only for certain values of X or Y (Figure 3c). Thus, depending on the phase of either X or Y, the amplitude of the driven component may increase/decrease when the cross-scale interaction takes place, and go back to normal when outside of the phase of the driving component.

145 This is a phase-amplitude interaction. In Figure 3b, Y_{PA} amplitude decreases when X is at its maximum (*i.e.* when its phase is a ridge, Figure 3c, top and middle panels, respectively). Similarly to the phase-phase interaction, $f_{PA}(t)$ is the difference between $X(t)$ and $Y_{PA}(t)$ (Figure 3c, bottom panel). Because phase amplitude are very dependent on inputs ϕ_X and ϕ_Y, connections between spatially distant physical processes are likely to give rise of phase-amplitude interactions (Nandi et al., 2019).

150 Following Paluš (2014) and (Jajcay et al., 2018), who compared the most used methods when studying causality, we choose the conditional mutual information (CMI) surrogates method, combined with wavelet transforms. First, using a Morlet mother wavelet, the instantaneous phase and amplitude at time t and scale s of the signal are obtained. Next, the conditional mutual

information, $I(\phi_x(t); \phi_y(t+\tau) - \phi_y(t)|\phi_y(t))$ for the phase and $I(\phi_x(t); A_y(t+\tau)|A_y(t)), A_y(t-\eta)), A_y(t-2\eta))$ for the amplitude is computed. In the case of phase-phase relationships, the CMI measures how much the present phase of x contains

155 information about the future phase of y knowing the present value of y. Phase-phase interactions can be uni- or bi-directional. It is possible for a single time scale to drive another, which in turn, drives back the original one, describing feedback interactions. For phase-amplitude relationships, CMI measures how much the present phase of x contains information of the future amplitude of y knowing the present and past values of y. The statistical significance of the CMI measure is assessed using 5000 phase-randomized surrogates, having the same Fourier spectrum, mean and standard deviation as the original time series, as

160 in Ebisuzaki (1997). Paluš (2014) has shown that this number of surrogates is ideal for statistical significance, in the context of hydroclimate time series. The computational cost is however high, with approximately one week of computing for a time series of 50 years, on a 32-core xeon computer. The present computations were done on the Myria cluster, hosted by the Centre Régional Informatique et d'Applications Numérique de Normandie (www.criann.fr).

3 Spatio-temporal clustering of hydrological variability

165 The wavelet transforms corresponding to each set of variables and each watershed have been computed and checked for similarities using IEDC fuzzy clustering to identify and characterize homogeneous regions of hydroclimate variability over France. Cross-scale couplings were then investigated for each homogeneous region.

3.1 Precipitation

3.1.1 Time-frequency patterns

170 Seven regions with homogeneous time-frequency patterns are identified (Figure 4a): North-western (green), North-eastern (blue), Centre-North (red), Centre-western (pink), Centre-eastern (black), South-western (yellow) and South-eastern (dark green). Based on fuzzy clustering, except for the Northern Alps regions, which show a mix of different regions (i.e. Centre-eastern, Centre-western, North-eastern, Centre-North and North-western), most regions are dominated by a spectral characteristic, defining a single member (*i.e.* cluster), suggesting a greater spatial coherence. Note that Centre-eastern, Centre-western,

175 North-eastern, Centre-North and North-western regions are characterized by mountainous ranges, where there is a significant part of solid precipitation, which may contribute to membership mixing, and weaker spatial coherence in those regions. Similarly, Northern regions are split between oceanic influence (to the west), inland (Centre) and mountainous ranges. Centre and Southern regions are delineated by mountain and valleys spatial extent (cf. Figure 1b).

In all regions, on average, precipitation is varying at different time scales, ranging from seasonal to inter-annual (i.e. 2-8

180 years; Figure 4b). Continuous wavelet spectra however show that those time scales of variability are non-stationary (Figure 4c), with temporal changes in terms of amplitude discriminating the different regions. For instance, South-western regions are characterized by quasi-continuous annual variability until the late 1980s, while other watersheds show sparsely significant annual variability (Figure 4c). Similarly, although there is significant inter-annual variability in all watersheds from the late

1980s, there is no significant inter-annual variability over the South-western and -eastern regions (Figure 4c). After removing
185 the seasonal cycle, focusing on inter-annual time scales, significant fluctuations at 4 and 8 years emerge for the South-western
and -eastern regions, but are much less pronounced and significant over shorter periods of time than in other regions (Figure
5).

In summary, different regions with coherent precipitation variability are identified, and are characterised by three time scales
of variability: intra-seasonal, annual and inter-annual. The amplitude of those time scales of variability however differs in time
190 and over French territory. The Northern-Alps appear much less coherent, and seems to share spectral characteristics with other
regions, especially those characterized by the presence of mountain ranges.

3.1.2 cross-scale interactions

Figure 6 shows cross-scale interactions for each cluster of precipitation variability (cf. Figure 4).

North-eastern, South-eastern, North-centre, North-western and Centre-eastern regions all show the phase of a 5-8yr vari-
195 ability driving the variability of smaller time scales (Figure 6a, blue, dark green, red, green, black, lower half of the graph).
This cross-scale interactions is however more pronounced in North-eastern and South-eastern regions (Figure 6a). Similarly,
eastern regions exclusively show $5 - 8yr \rightarrow 2 - 4yr$ interactions, while other regions show self-interacting 5-8yr variability
(Figure 6a). The upper half of the graph, which refers to higher-frequency driving lower-frequency variability, is populated
by North-centre, South-eastern, North-western and North-eastern regions (Figure 6a, red, dark green, green and blue). South-
200 eastern shows cascade phase-phase interactions, $i.e.$ $2 - 3yr \rightarrow 5 - 4yr \rightarrow 6 - 5$ (Figure 6a, dark green). In addition, both
South-eastern and North-western regions show mirror interactions with their lower half counterparts, $e.g.$, $5 - 6yr \leftrightarrow 4 - 5yr$
(Figure 6a, dark green, green mirror patches about the diagonal). We also note that phase-phase interactions are very weak over
the South-western regions, and absent in the centre-western regions.

Phase-amplitude interactions are presented in Figure 6b. The lower half of the graph, which refers to lower-frequency driving
205 higher-frequency variability, is populated by $5 - 8yr \rightarrow 2 - 4yr$ interactions for western and North-centre regions (Figure
6b, pink, yellow, green, red). Centre-eastern regions are also showing lower-frequency variability driving higher-frequency
variability, between $8yr \rightarrow 6yr$ variability (Figure 6b). Notably, the North-western region is the only one with cross-scale
interactions driving the annual cycle (Figure 6a, green).In the upper half of the graph, which refers to higher-frequency driving
lower-frequency variability, we only find North-centre and North-eastern regions, showing $2 - 4 \rightarrow 4yr$ and $3 - 4yr \rightarrow 7 - 8yr$
210 phase-amplitude interactions (Figure 6b, blue, red). Note that North-centre, North-eastern and Centre-eastern regions show
phase-amplitude and phase-phase interactions at very similar time scales (Figure 6a,b, red, blue, black), while time scales of
phase-amplitude and phase-phase interactions do not match in Centre-western and North-western and South-western regions
(Figure 6a, b, pink, green, yellow). Regions to the East thus appear to have both phase-phase and phase-amplitude interactions
at the same time scales, while western regions are more characterized by phase-amplitude interactions.

215 The precipitation cross-scale interactions can be of different forms: phase-phase, phase-amplitude, uni- or bi-directional,
from lower to higher time scales and vice versa. The presence of cross-scale interactions seems to be tied to specific spatial
locations, suggesting different internal dynamics, over the different regions of homogeneous precipitation variability. Inter-

estingly, cross-scale interactions tend to converge toward specific time scales, 2-4yr and 5-8yr, which were linked to ocean-atmosphere variability, such as the North Atlantic Oscillation, in previous hydroclimate studies over France (Feliks et al., 2011;

220 Fritier et al., 2012; Dieppois et al., 2016; Massei et al., 2017). However, the presence of mirror interactions also indicate strong bidirectional negative feedback, which might refer to interaction between ocean-atmospheric variability and land-surface processes (Mariotti et al., 2018). Soil moisture has been shown to be either a positive or negative feedback while several negative feedbacks have been identified in both ocean-atmosphere and land-ocean interactions (Boé, 2013; Sejas et al., 2014).

3.2 Temperature

225 ### 3.2.1 Time-frequency patterns

In temperature, nine regions with homogeneous time-frequency patterns are identified (Figure 7a): North-western-high (pink), North-western-low (black), North-eastern (blue), Centre-eastern (red), Centre-western (green), South-eastern-high (yellow), South-eastern-low (brown), South-western-high (dark green) and South-western-low (purple). Fuzzy clustering shows that watersheds typically converge toward singular clusters, defining highly coherent regions (Figure 7a). This is however not true

230 for the Centre-western region, which is characterized by a mix of spectral characteristic defining other regions (cf. red, green, black, yellow and purple pie charts, Figure 7a).

Using monthly data, temperature is primarily varying on an annual time scale, with very similar amplitudes for all regions (Figure 7b-c). However, differences between those regions can be explained by temporal changes in inter-annual variability, which can only be significantly detected after removing the seasonal cycle (Figure 8a-b). Focusing on inter-annual variability,

235 significant temperature variations indeed emerge at 2-4yr and 5-8yr time scales, and show different timings and amplitudes over the different regions (Figure 8a-b). All regions show 5-8yr variability, but southern regions show significantly higher amplitude of the 2-4yr variability than northern regions (Figure 8a). Similarly, While stronger 2-4yr variability variability occur in the 1980s and 1990s in the South-western-low region, other regions show significant 2-4yr variability from the 2000s, only (brown, Figure 8b).

240 ### 3.2.2 cross-scale interactions

Figure 9 shows cross-scale interactions for each cluster of temperature variability identified in Figure 8a.

For temperature, phase-phase interactions are mostly concentrated in the upper half of the graph, which refers to higher-frequency modulating lower-frequency (Figure 9a). Notably, a $2-6yr \rightarrow 6-8yr$ phase-phase interaction appears more pronounced over Northern regions (Figure 9a, blue, red, pink, black). The Centre-western region shows similar phase-phase

245 interactions, but at $1-3yr \rightarrow 4-6yr$ time scales (Figure 9a, green). In the lower half of the graph, which refers to lower-frequency modulating higher-frequency, interactions are found at very similar timescales, but at slightly higher frequency, for all regions (e.g. , $2-5yr \rightarrow 1-4yr$ variability). Temperature in the South-western-low region, however, show slightly different characteristics, phase-phase interactions between lower- and higher-frequency occurring between $7-8yr \rightarrow 3-4yr$ and $7-8yr \rightarrow 3-4yr$ variability (Figure 9a, purple).

250   Temperature phase-amplitude interactions are mostly acting on the 3-4yr time scale for all regions (Figure 9b). In particular, in temperature, more pronounced phase-amplitude interactions are found over the South-western-low region (Figure 9b, purple), which consistent with previous studies on phase-amplitude interactions in European temperature (Palus, 2014; Jajcay et al., 2016). Over South-western regions, temperature, however, shows both $3-8yr \rightarrow 3-4yr$ and $2-4yr \rightarrow 4-7yr$ phase-amplitude interactions (Figure 9b, brown, purple). Furthermore, it should be noted that temperature variability interactions

255   occur between very similar time scales over a number of regions (Figure 9b, pink, red, yellow, purple). According to Paluš (2014), interactions between very similar times, or the same times, can only occur if, at least, two processes are present.

As for precipitation, phase-phase and phase-amplitude cross-scale interactions are region-dependent, and can be uni- or bi-lateral, in temperature. However, in temperature, most phase-phase interactions occur from higher- to lower-frequency variability, while phase-amplitude interactions tend to occur from lower- to higher-frequency variability. Similarly, while time

260   scales involved for phase-phase and phase-amplitude interactions are very similar in precipitation, they differ largely in temperature (Figure 9b). This suggests that the processes driving phase-phase and phase-amplitude cross-scale interactions are different in temperature, and also different between temperature and precipitation. As previously suggested for precipitation, such cross-scale interactions might refer to negative feedbacks between ocean, atmosphere and land-processes, which can be noticeably different in temperature. Temperature variability is mostly derived from changes in heat advection from the North-

265   Atlantic oceans over most of the French territory, except for the Mediterranean regions that are strongly influenced by the Mediterranean Sea (Scherrer, 2006; Sodemann and Zubler, 2010). In addition, temperature's feedback processes (*i.e.* positive or negative) are extremely region-dependent (Lorenz et al., 2016; Levine et al., 2016; Levine, 2019). Nevertheless, such feedback processes could result from regional changes in soil moisture, as well as from heat exchanges between ocean and land, especially over the coastal regions (Lambert et al., 2011; Sejas et al., 2014).

270   3.3   Discharge

3.3.1   Time-frequency patterns

Six regions with homogeneous time-frequency patterns are identified in discharge (Figure 10a): North-western (black), North-eastern (blue), North-Centre (red), Centre-western (green), South-eastern (yellow) and South-western (pink). However, several watersheds, especially in the South, show memberships to multiple regions, suggesting lower spatial coherence in discharge

275   than in precipitation and temperature. Lower spatial coherence, however, could mostly be explained by mixing of solid and liquid precipitation in driving discharge variability in the Alps and from the local heterogeneity of precipitation due to convective dynamics in the Pyrenees. Nevertheless, the number of significant homogeneous regions is lower in discharge than in precipitation and temperature, and northern regions are particularly coherent.

Using monthly data, discharge is mainly varying on annual time scales, as determined through the global wavelet spectra (Figure 10b). Unlike other regions, South-eastern watersheds, however, shows significant intra-seasonal variability, even

280   using monthly data (Figure 10b). Continuous wavelet spectra show that both annual and intra-seasonal variability can be non-stationary, with temporal changes in terms of amplitude discriminating the different homogeneous regions of discharge

variability (Figure 10c). For instance, annual variability is only significant for specific periods in the South-eastern watersheds, while other regions show mostly constant annual variability (Figure 10c). Similarly, in the South-eastern region, intra-seasonal

285   discharge variability sparsely appears significant from the 1980s, absent from the other regions (Figure 10b).

After removing the seasonality, focusing on inter-annual variability, North-eastern watersheds stand out as having continuous significant inter-annual variability throughout the time series, with 4-5yr and 5-8yr variability before and after the 1990s, respectively (Figure 11b). South-eastern and -western regions also stand out, as they show 2-4yr variability in the mid-1970s and 2000s (Figure 11b, yellow, pink). In addition, South-eastern regions do not show significant variability in discharge at time

290   scales greater than 4yr (Figure 11a-b).

Different coherent regions are thus identified for discharge variability. In addition, these homogeneous regions correspond well with regions identified in precipitation and temperature variability. As in precipitation and temperature, those regions seem strongly impacted by the presence of mountain ranges (cf. Figure 1b). However, compared to precipitation and temperature, southern regions, which may appear more complex in term of climate and its link to land-surface processes, appear much less

295   spatially coherent in discharge.

3.3.2   cross-scale interactions

A major question concerning discharge cross-scale interactions is whether interactions found in either precipitation or temperature are also present in discharge. Phase-phase interactions that were found in precipitation are also identified in discharge, in particular over North-eastern, South-eastern and North-western regions (blue, yellow and black; Figure 6a, Figure 12a).

300   Phase-phase interactions that were identified in temperature are much less evident (Figure 9a, Figure 12a). It should also be noted that many small patches, describing phase-phase interactions in precipitation and temperature, are systematically not transferred to discharge variability (Figures 6a, 9a, 12a). Instead, discharge variability seems to exclusively preserve large patches of phase-phase interactions(Figures 6a, 9a, 12a), suggesting that catchment properties are modulating the climatic signals (i.e. precipitation and temperature). Such filtering of climate signals is even more pronounced in certain regions, such

305   the North-centre, where phase-phase interactions are absent in discharge (Figure 12a), but were identified in precipitation and temperature (Figure 6a, 9a).

But, more importantly, there is no phase-amplitude interaction in discharge (Figure 12b). This points out that watershed properties modulate the interacting processes in precipitation and temperature. Since phase-amplitude interactions require a negative feedback system, any change of the feedback sign (by either runoff or subsurface processes) can cancel those

310   phase-amplitude interactions. As our data set is mostly composed of low groundwater support, those modulations are unlikely to results from the water table, especially as phase-phase interactions are inherited from precipitation. In addition, further analysis on Paris' Austerlitz gauging station, which includes very large groundwater support, reveals the same absence of phase-amplitude interaction in discharge (not shown, Flipo et al. (2020)). Possible explanations include the frequency partitioning of watershed compartments or integration process along the river network breaks any spatial connection and thus smooths out

315   and flattens phase-amplitude interactions (Schuite et al., 2019).

cross-scale interactions are only of phase-phase nature in discharge. All phase-phase interactions in discharge seem to be primarily related to precipitation, even though the strong correlations between rainfall and temperature makes it difficult to detect. However, differences between regions of homogeneous discharge variability are very similar to those detected in precipitation. Further work is however needed to understand why phase-amplitude cross-interactions are absent in discharge

320 variability. Catchment properties appear to involve positive rather than negative feedback, thus resulting in a loss of phase-amplitude interactions.

4 Discussions an conclusions

As recommended by Blöschl et al. (2019), studying the different scales of spatial and temporal variability, as well as their interactions, remains one of the most important challenges in hydrology. In this study, we unravelled homogeneous regions

325 of hydroclimate variability in France, accounting for non-stationarity and non-linearity, bringing additional information over previous, regime-based, classifications in France or elsewhere (Champeaux and Tamburini, 1996; Bower and Hannah, 2002; Sauquet et al., 2008; Snelder et al., 2009; Joly et al., 2010; Gudmundsson et al., 2011). This was achieved through a clustering analysis based on time-frequency patterns of precipitation, temperature and discharge variability over 152 watersheds. We then studied the spatio-temporal characteristics of each homogeneous region, including characteristic time scales of hydroclimate

330 variability (i.e. precipitation, temperature and discharge) and cross-scale interactions.

Our study reveals different coherent regions of precipitation, temperature and discharge variability. Yet, some watersheds are characterized by a mix of spectral characteristics from surrounding regions, or regions with the same topographic characteristics. Those coherent regions are homogeneously distributed over France in precipitation and discharge, but show large discrepancies in term of spatial extension in temperature. According to previous clustering of hydroclimate variability over

335 France, Northern regions are more homogeneous than what was found here (Champeaux and Tamburini, 1996; Sauquet et al., 2008; Snelder et al., 2009; Joly et al., 2010), and show lower spatial coherence. In particular, here, we demonstrate that both the amplitude and timings of the different time scales of hydroclimate variability differentiate the regions, highlighting the need for accounting for non-stationary behaviours in global to regional hydroclimate study. Overall, hydroclimate variability displays intra-seasonal (<1yr), annual (1yr) and inter-annual (2-4yr and 5-8yr) time scales. Our results, which were focused on

340 the French territory, are therefore consistent with time scales of variability identified over the world major rivers (Labat, 2006).

Looking at the internal dynamics of each coherent region, i.e. phase-phase and phase-amplitude causal relationships, complex interactions have been identified. Those interactions can be orientated from lower (higher) to higher (lower) time scales of variability, can be uni- or bi-directional and even self-interacting. For all regions, even regions with very similar time-frequency patterns, the cross-scale interactions are very different, which implies different internal dynamic (Paluš, 2014). As suggested

345 earlier, this might also highlight different interactions between ocean, atmosphere and land-surface processes over the different regions of France. For instance, the interactions between atmosphere variability (either precipitation or temperature) are known to be strongly modulated by interactions with land-surface processes, such as soil moisture, evapotranspiration, and surface albedo (including snow and ice cover), and these processes are more or less important over the French territory

(Ducharne et al., 2020). But more importantly, phase-phase interactions in discharge variability appear partly inherited from
350 precipitation and temperature. This suggests that the watershed characteristics do not entirely filter the interactions between
ocean, atmosphere and land-processes driving precipitation and temperature. Interestingly, however, discharge variability does
not show any phase-amplitude causality, while such interactions are significant in precipitation and temperature. This suggests
that catchment properties substantially modulate the amplitude of the input climate signal (i.e. precipitation and temperature),
which are then not transferred to discharge variability. Such finding is consistent with previous studies, showing that infiltration
355 processes and ground water variability acts as a low-pass filter on the input precipitation and temperature variability (Massei
et al., 2007). However, our hydrological data set contains very few watersheds with groundwater support. The processes driving
those amplitude modulations could not be fully explained within the scope of this study, and require further explorations.

Nevertheless, those findings allow for a better identification of climate deterministic processes controlling hydroclimate
variability, notably using cross-scale analysis, which could help identifying more robust climate drivers. For instance, it is
360 important to discriminate pure climate influence from climate-land processes interactions. This has large implications for
seamless hydrological predictions based on climate information, as only some parts of the climate signals are transferred
to discharge systems. Thus, causal cross-scale relationship could be used to inform and improve existing seasonal to multi-
year seamless forecasting for hydrological variability, including extremes (e.g. flood and drought). Preliminary work in this
direction were recently proposed by Jajcay et al. (2018), who developed a composite binning method enabling to forecast a
365 particular time series based on conditional phase of another. Similarly, it would be of crucial importance to determine whether
hydrological models, which are commonly used in climate-impact assessments, are reproducing the filtering-processes induced
by the catchment properties, and identify those (Ducharne et al., 2020). Long term hydroclimate variability only represents a
fraction of the total variability, however, strong teleconnections between long term and smaller than inter-annual time scales
have been highlighted. Those teleconnections result from both spatial and temporal interactions and feedback between the
370 hydroclimate processes (Feliks et al., 2016). Owing to the recent addition of long term, high spatial resolution hydroclimate
data sets (e.g. Fyre reconstructions, Devers et al. (2020, 2021)) it is now possible to apply the clustering and cross-scale analyses
to better characterize the effects that long term hydroclimate variability (e.g. multi-decadal) has on smaller time scales. The
methodology presented in this work can enable deeper analyses than those based on correlations, which may overlook some
important hydroclimate processes.
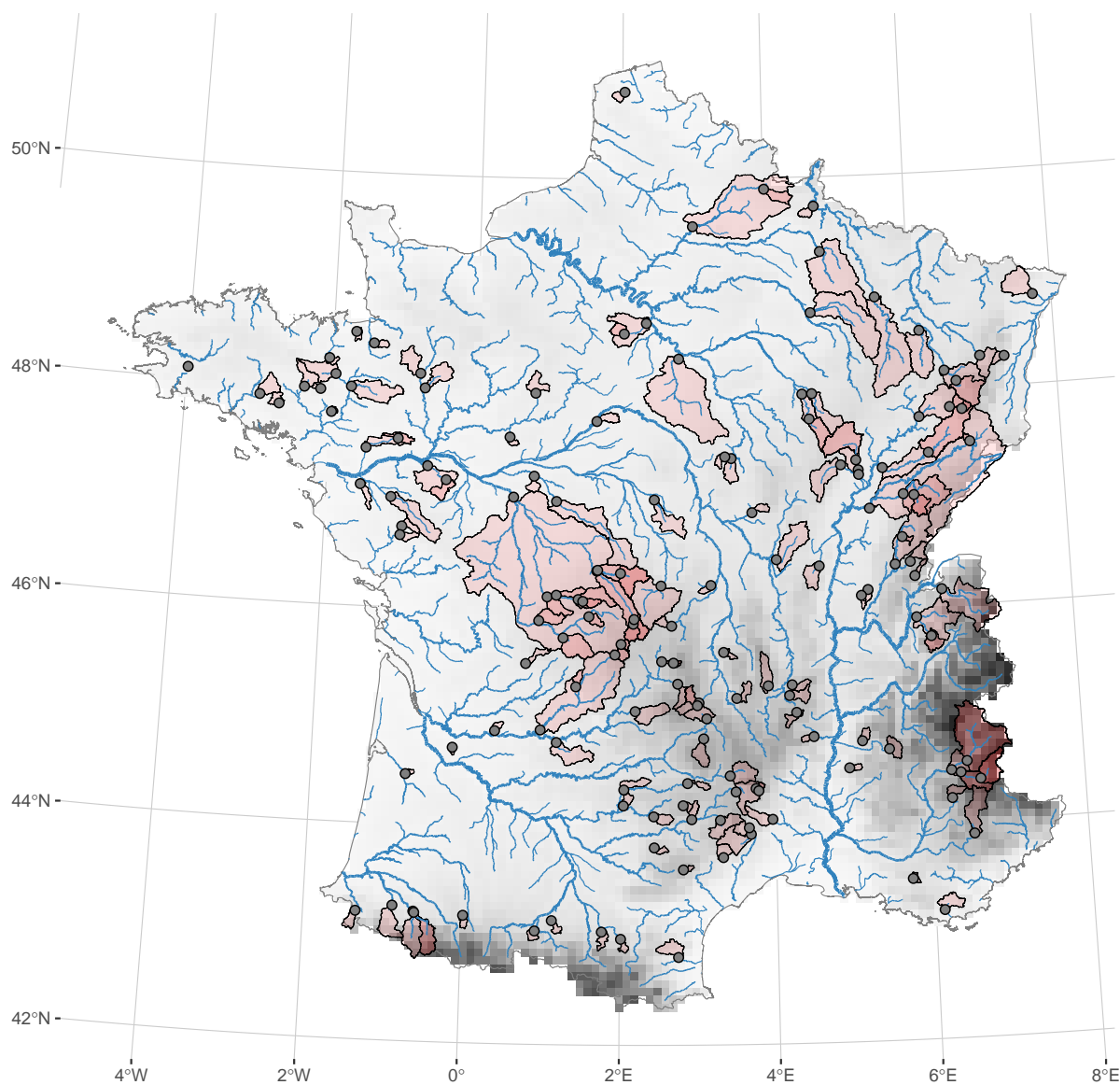
Figure 1. Location of stream gauges (grey dots), corresponding watersheds (pale red, Brigode et al. (2020)), hydrographic network (blue lines, Pella et al. (2012)), and orography in Safran dataset (grey scale, Vidal et al. (2010)).
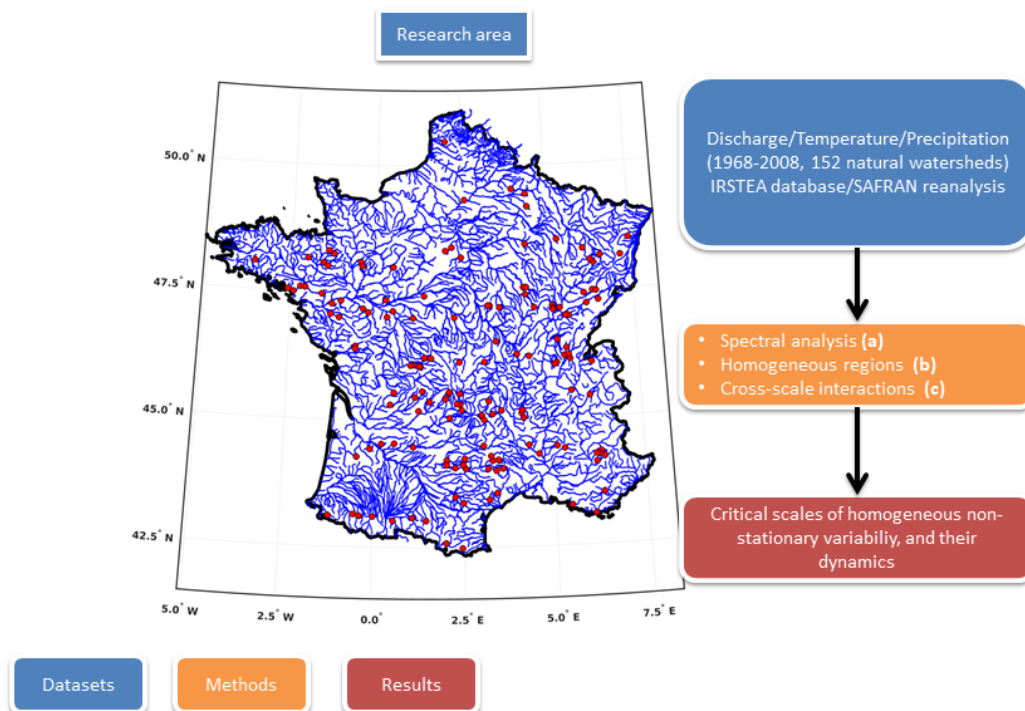
Figure 2. Workflow of this study. (**a**) 152 monthly precipitation, temperature and discharge time series are extracted from IRSTEA's watershed database. The following steps are applied to each variable. (**b**) the continuous wavelet spectrum for each watershed is computed. (**c**) A distance matrix between wavelet spectra is then established; d.) A fuzzy clustering algorithm is used to build a classification map of the watersheds based on their wavelet spectra.
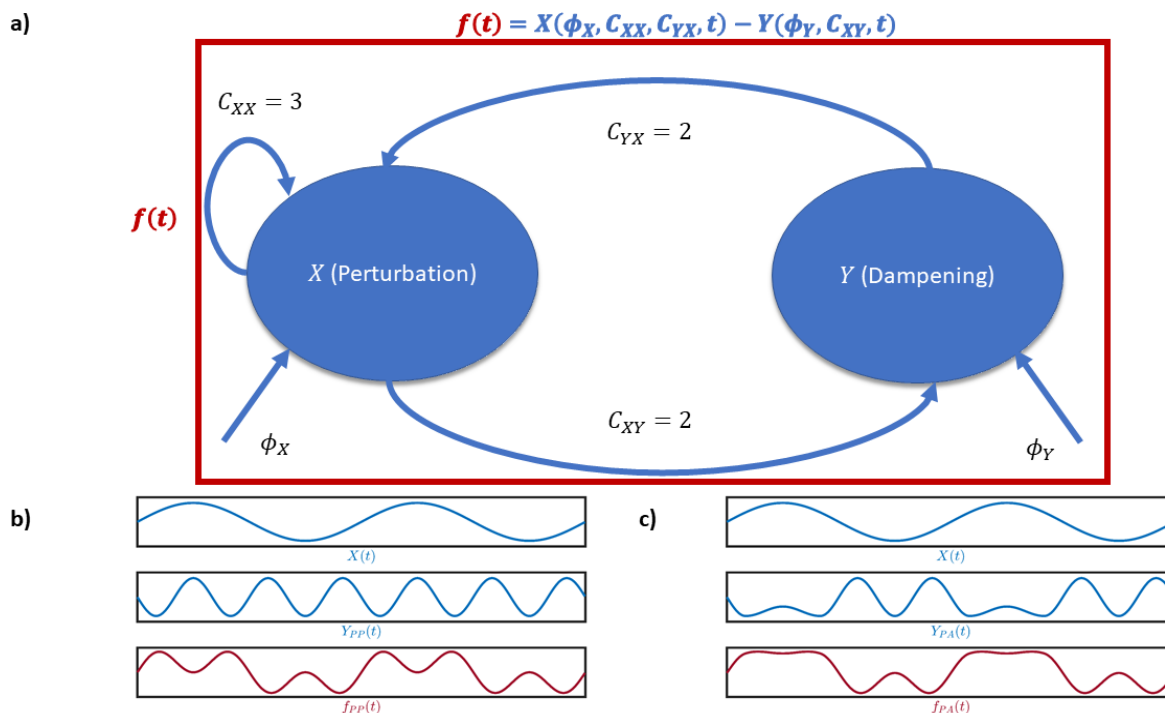
Figure 3. A system with directional cross scale interactions. **a)** A variable $f(t)$ made of two components X and Y, connected through C_{XY} and C_{YX} in a perturbation-dampening scheme so that $f(t) = X(t) - Y(t)$. Both X and Y receive inputs ϕ_X and ϕ_Y, respectively. C_{XX} allows X to grow first. Depending on both inputs and connections, some phase-phase or phase-amplitude interactions between X and Y can occur. **b)** an example of a phase-phase interaction, with every fourth ridge of Y_{PP} coinciding with a ridge of X, with $f_{PP}(t) = X(t) - Y_{PP}(t)$ (top, middle and bottom panels, respectively). **c)** an example of phase-amplitude interaction. X and Y_{PA} only interact when X reaches a ridge, in which case Y_{PA} amplitude if lowered, yielding $f_{PA}(t)$ (Top, middle and bottom panels, respectively). (adapted from Onslow et al. (2014))
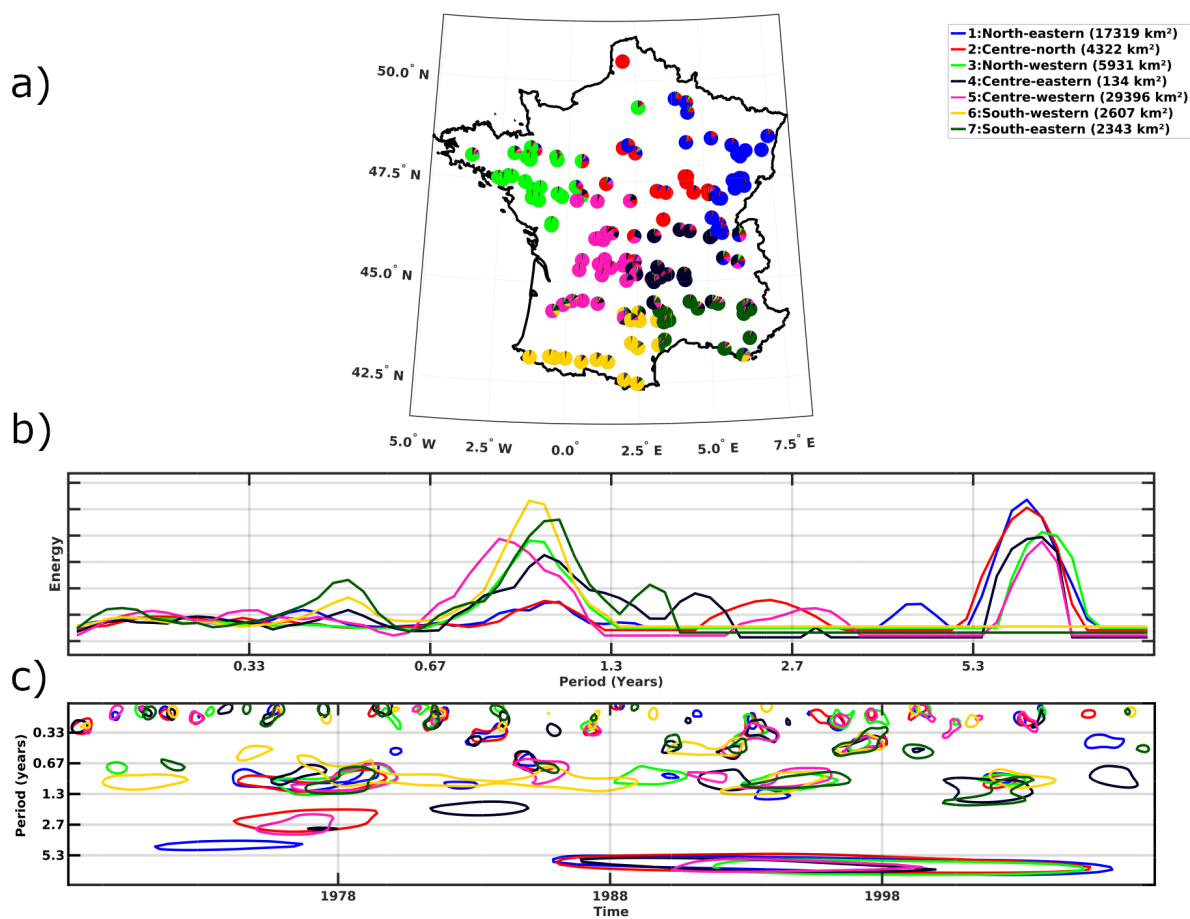
Figure 4. Clustering of precipitation time-frequency variability in France. (**a**) Classification map of the watersheds. Pie charts slices show the three highest probability memberships. Pie charts denote fuzzy clustering memberships. (**b**) Global wavelet spectra for each cluster (95% significance level against red noise). (**c**) Statistically significant wavelet spectra for each cluster.
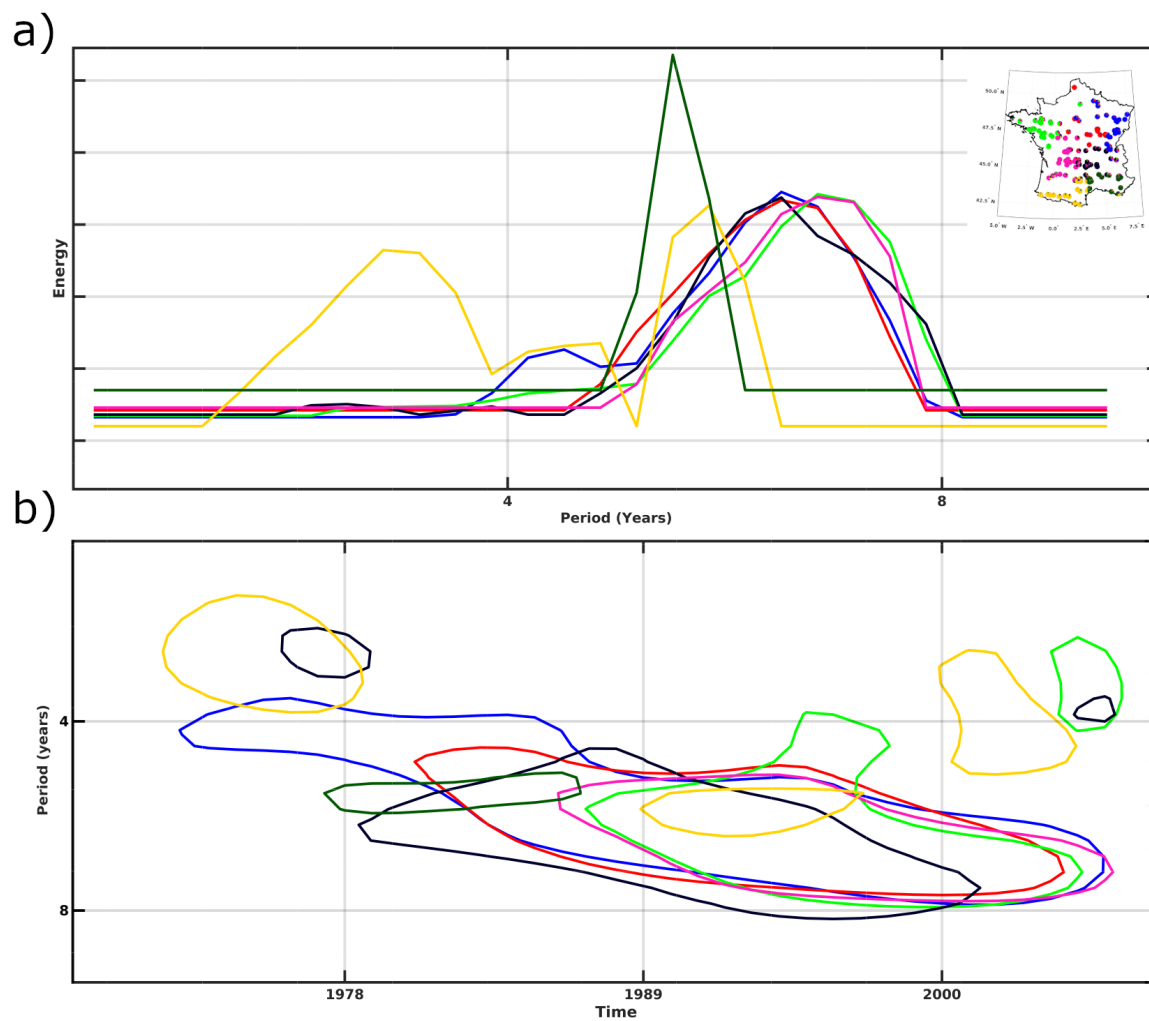
Figure 5. Inter-annual precipitation time-frequency variability in France. (**a**) Global wavelet spectra for each cluster. (**b**) Statistically significant (95% significance level) wavelet spectra for each cluster.

a)
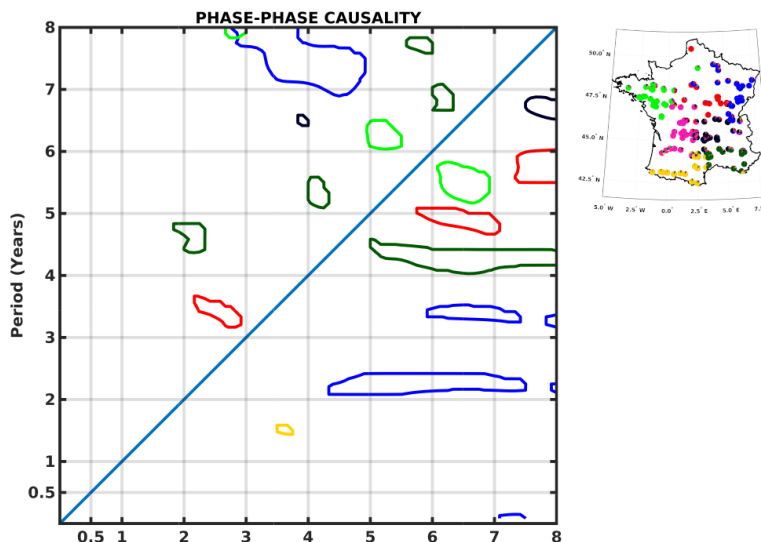
b)
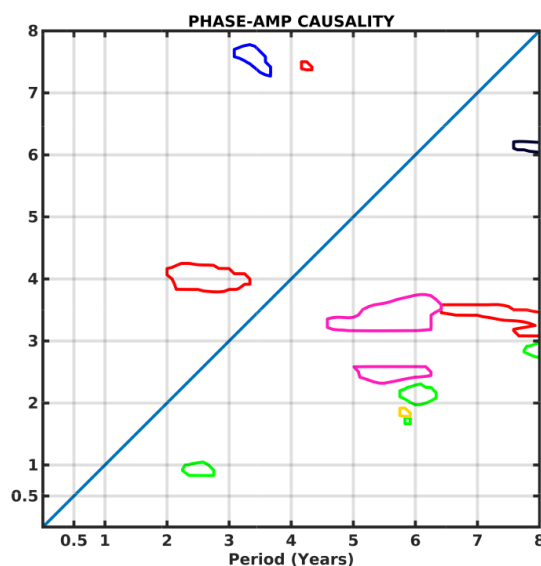
Figure 6. Precipitation cross-scale interactions (95% significance level).The driving time scale is on the horizontal axis, the driven on the vertical axis (*i.e.* the time scale x phase has a causal relationship with the phase/amplitude of the driven time scale y). Lower(upper) half of the graph, below (above) the diagonal, show time scales acting on smaller (larger) time scales. (**a**) Phase-phase causality. (**b**) Phase-amplitude causality.
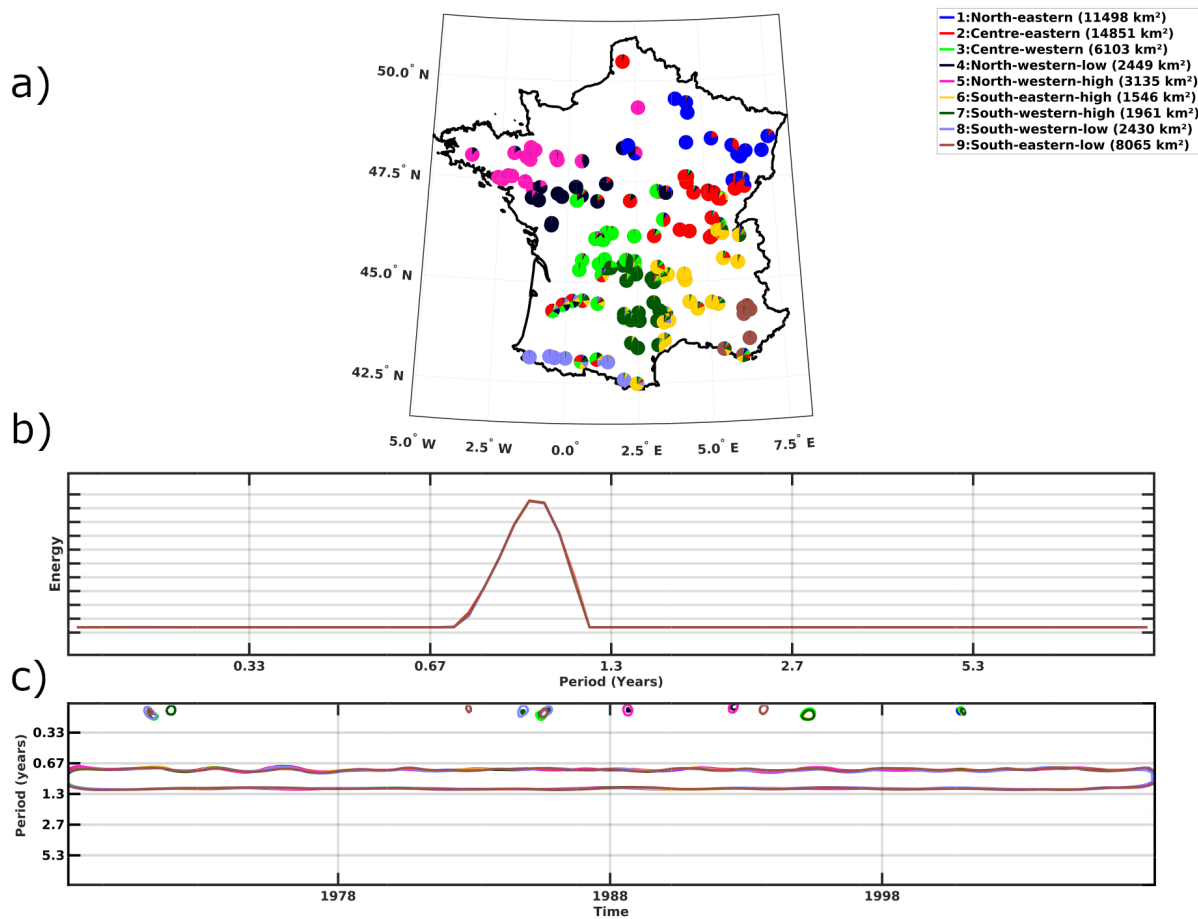
Figure 7. Clustering of temperature time-frequency variability in France. (**a**) Classification map of the watersheds. Pie charts slices show the three highest probability memberships (**b**) Global wavelet spectra for each cluster. (**c**) Statistically significant wavelet spectra for each cluster.
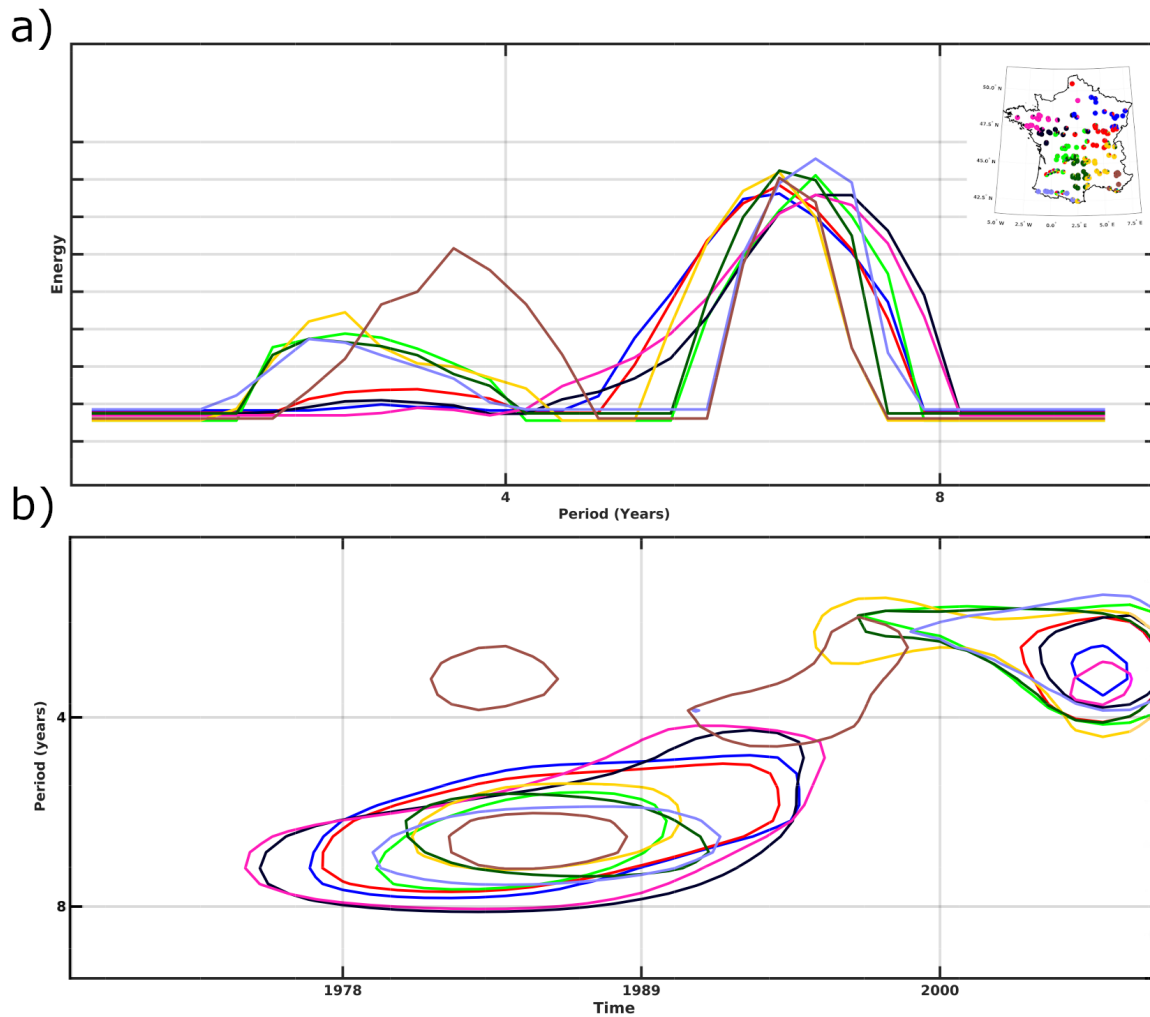
Figure 8. Inter-annual temperature time-frequency variability in France. (**a**) Global wavelet spectra for each cluster. (**b**) Statistically significant wavelet spectra for each cluster.

a)
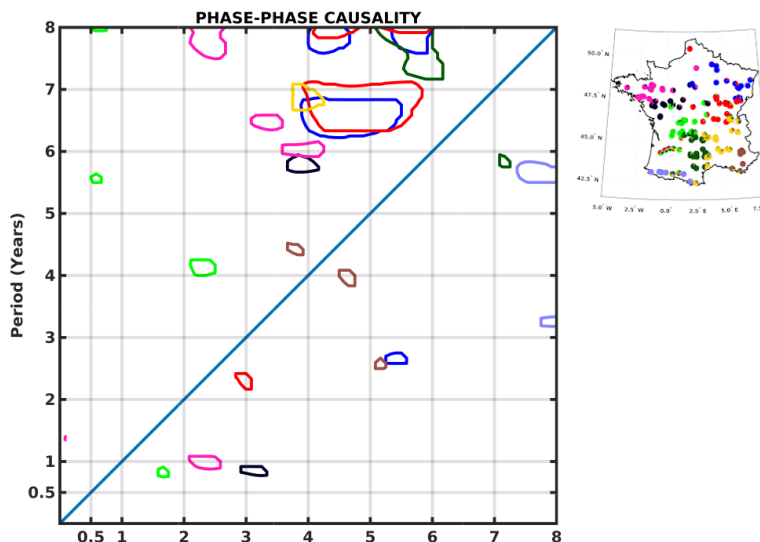
b)
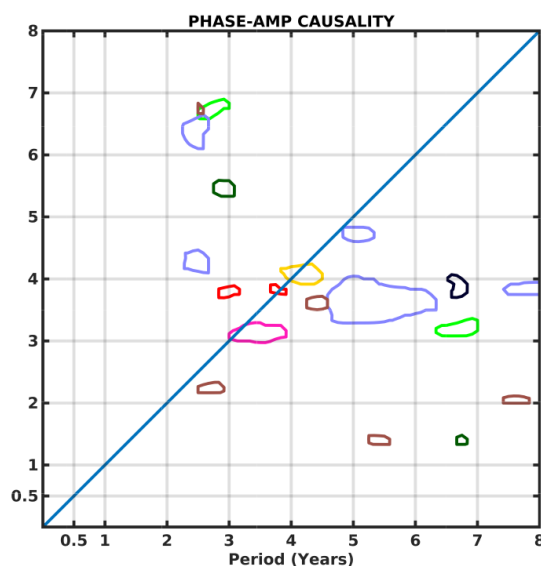
Figure 9. Temperature cross-scale interactions (95% significance level).The driving time scale is on the horizontal axis, the driven on the vertical axis (*i.e.* the time scale x phase has a causal relationship with the phase/amplitude of the driven time scale y). Lower(upper) half of the graph, below (above) the diagonal, show time scales acting on smaller (larger) time scales. (**a**) Phase-phase causality. (**b**) Phase-amplitude causality
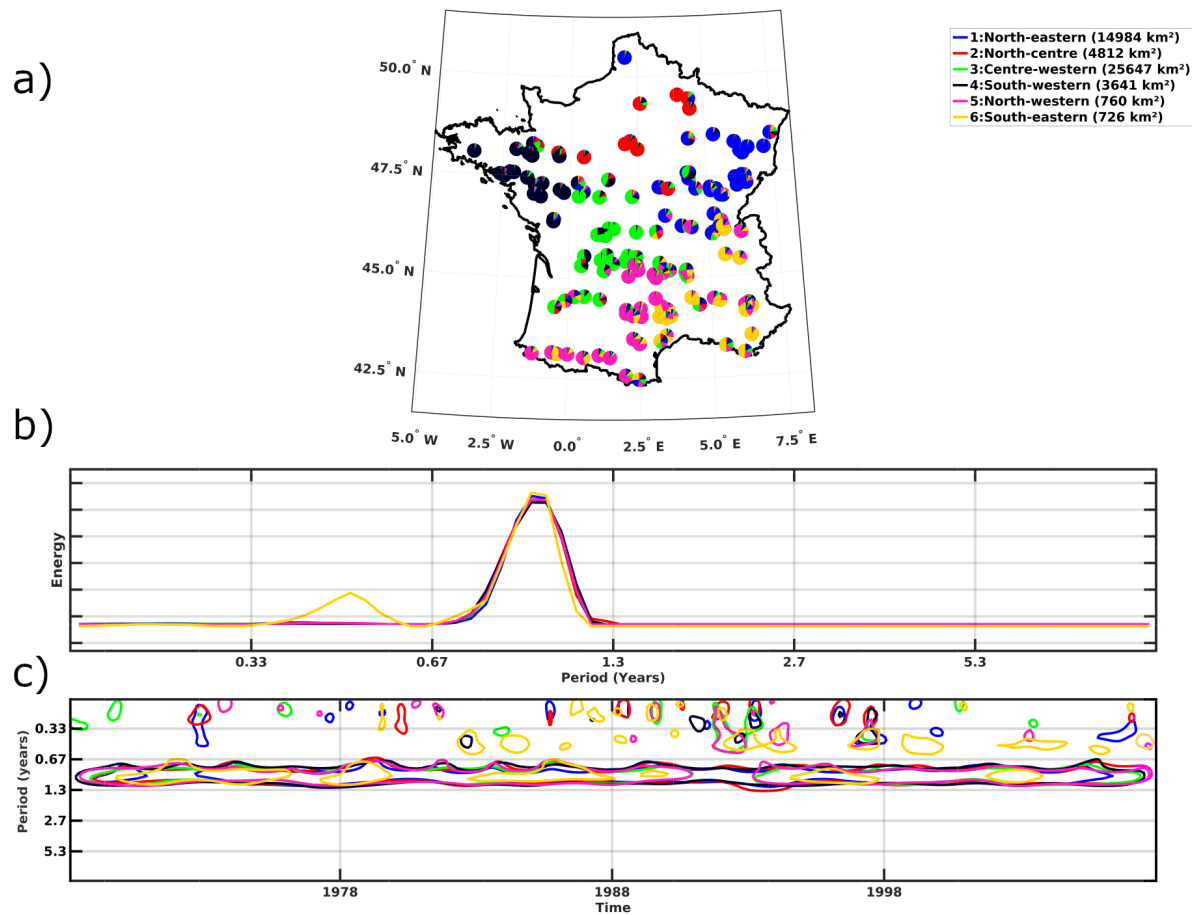
Figure 10. Clustering of discharge time-frequency variability in France. (**a**) Classification map of the watersheds. Pie charts slices show the three highest probability memberships (**b**) Global wavelet spectra for each cluster. (**c**) Statistically significant wavelet spectra for each cluster.
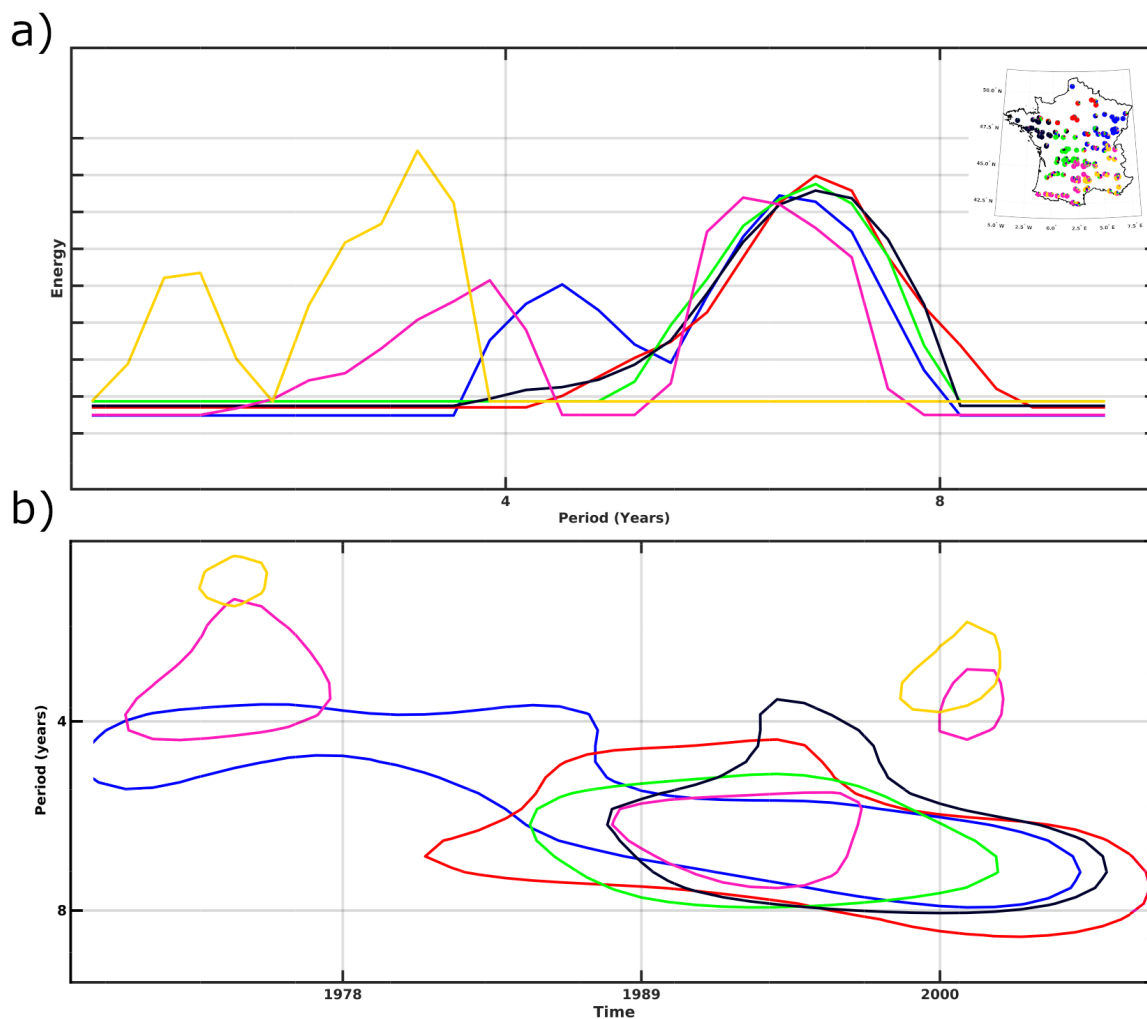
Figure 11. Inter-annual discharge time-frequency variability in France. (**a**) Global wavelet spectra for each cluster. (**b**) Statistically significant wavelet spectra for each cluster.

a)
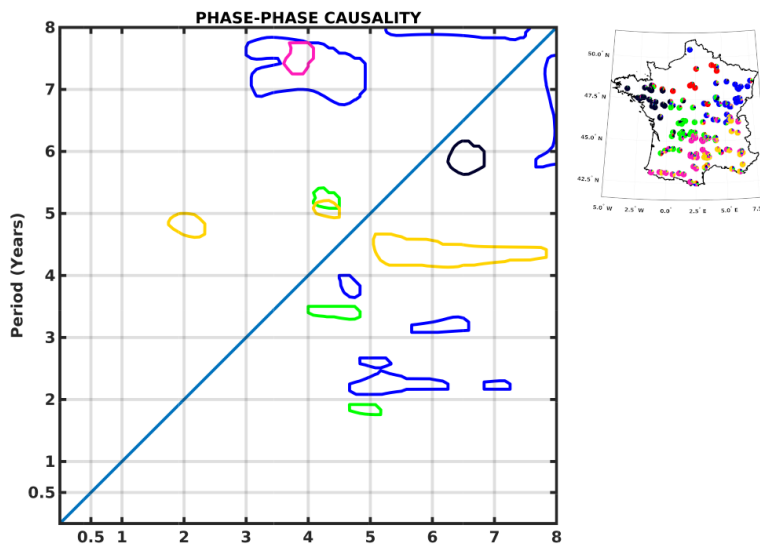
b)
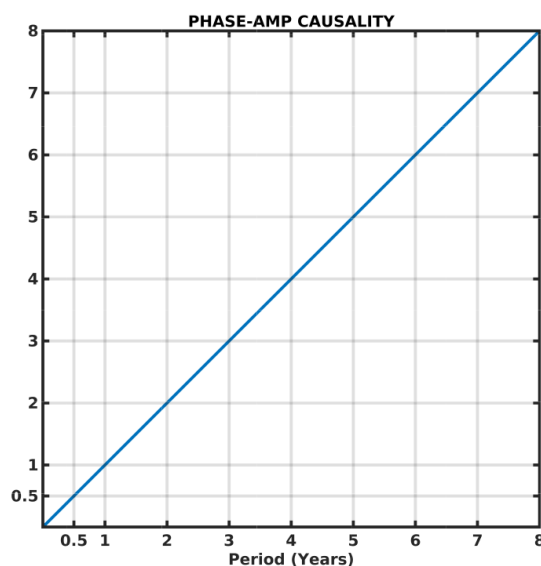
Figure 12. Discharge cross-scale interactions (95% significance level).The driving time scale is on the horizontal axis, the driven on the vertical axis (*i.e.* the time scale x phase has a causal relationship with the phase/amplitude of the driven time scale y). Lower(upper) half of the graph, below (above) the diagonal, show time scales acting on smaller (larger) time scales. (**a**) Phase-phase causality. (**b**) Phase-amplitude causality

References

Anctil, F. and Coulibaly, P.: Wavelet Analysis of the Interannual Variability in Southern Québec Streamflow, Journal of Climate, 17, 163–173, 2004.

Blöschl, G., Bierkens, M. F. P., Chambel, A., Cudennec, C., Destouni, G., Fiori, A., et al.: Twenty-three Unsolved Problems in Hydrology (UPH) – a community perspective, Hydrological Sciences Journal, 0, 1–33, https://doi.org/10.1080/02626667.2019.1620507, 2019.

Boé, J.: Modulation of soil moisture-precipitation interactions over France by large scale circulation, Climate Dynamics, 40, 875–892, https://doi.org/10.1007/s00382-012-1380-6, 2013.

Bower, D. and Hannah, D. M.: Spatial and temporal variability of UK river flow regimes, IAHS-AISH Publication, pp. 457–466, 2002.

Brigode, P., Génot, B., Lobligeois, F., and Delalgue, O.: Summary sheets of watershed-scale hydroclimatic observed data for France, https://doi.org/Summary sheets of watershed-scale hydroclimatic observed data for France, https://webgr.inrae.fr/activites/base-de-donnees/, 2020.

Caillouet, L., Vidal, J. P., Sauquet, E., Devers, A., and Graff, B.: Ensemble reconstruction of spatio-temporal extreme low-flow events in France since 1871, Hydrology and Earth System Sciences, 21, 2923–2951, https://doi.org/10.5194/hess-21-2923-2017, 2017.

Champeaux, J.-l. and Tamburini, A.: Zonage climatique de la France à partir des séries de précipitations (1971-1990) du réseau climatologique d'Etat, La météorologie, 8, 44–54, 1996.

Coulibaly, P. and Burn, D. H.: Wavelet analysis of variability in annual Canadian streamflows, Water Resources Research, 40, 1–14, https://doi.org/10.1029/2003WR002667, 2004.

Devers, A., Vidal, J. P., Lauvernet, C., Graff, B., and Vannier, O.: A framework for high-resolution meteorological surface reanalysis through offline data assimilation in an ensemble of downscaled reconstructions, Quarterly Journal of the Royal Meteorological Society, 146, 153–173, https://doi.org/10.1002/qj.3663, 2020.

Devers, A., Vidal, J.-p., Lauvernet, C., and Vannier, O.: FYRE Climate : A high-resolution reanalysis of daily precipitation and temperature in France from 1871 to 2012, Climate of the Past, https://doi.org/https://doi.org/10.5194/cp-2020-156, 2021.

Dieppois, B., Durand, A., Fournier, M., and Massei, N.: Links between multidecadal and interdecadal climatic oscillations in the North Atlantic and regional climate variability of northern France and England since the 17th century, Journal of Geophysical Research Atmospheres, 118, 4359–4372, https://doi.org/10.1002/jgrd.50392, 2013.

Dieppois, B., Lawler, D. M., Slonosky, V., Massei, N., Bigot, S., and Fournier, M.: Multidecadal climate variability over northern France during the past 500 years and its relation to large-scale atmospheric circulation, International Journal of Climatology, 36, 4679–4696, https://doi.org/10.1002/joc.4660, 2016.

Ducharne, A., Arboleda-obando, P., and Cheruy, F.: Effets de l'humectation des sols par les nappes sur la trajectoire du changement climatique dans le bassin de la Seine et en Europe, Tech. rep., PIREN-Seine, 2020.

Dunn, J. C.: A Fuzzy Relative of the ISODATA Process and Its Use in Detecting Compact Well-Separated Clusters A Fuzzy Relative of the ISODATA Process and Its Use in Detecting Compact Well-Separated Clusters, Journal of Cybernetics, 3, 37–57, 1973.

Ebisuzaki, W.: A Method to Estimate the Statistical Significance of a Correlation When the Data Are Serially Correlated, Journal of Climate, 10, 2147–2153, 1997.

Feliks, Y., Ghil, M., and Robertson, A. W.: The atmospheric circulation over the North Atlantic as induced by the SST field, Journal of Climate, 24, 522–542, https://doi.org/10.1175/2010JCLI3859.1, 2011.

Feliks, Y., Robertson, A. W., and Ghil, M.: Interannual variability in north Atlantic weather: Data analysis and a quasigeostrophic model, Journal of the Atmospheric Sciences, 73, 3227–3248, https://doi.org/10.1175/JAS-D-15-0297.1, 2016.

Flipo, N., Gallois, N., Labarthe, B., Baratelli, F., Viennot, P., Schuite, J., et al.: Pluri-annual Water Budget on the Seine Basin: Past, Current and Future Trends, in: Handbook of environmental chemistry, Springer, https://doi.org/10.1007/698_2019_392, 2020.

415 Fritier, N., Massei, N., Laignel, B., Durand, A., Dieppois, B., and Deloffre, J.: Links between NAO fluctuations and inter-annual variability of winter-months precipitation in the Seine River watershed (north-western France), Comptes Rendus - Geoscience, 344, 396–405, https://doi.org/10.1016/j.crte.2012.07.004, 2012.

Gentine, P., Troy, T. J., Lintner, B. R., and Findell, K. L.: Scaling in Surface Hydrology: Progress and Challenges, Journal of Contemporary Water Research and Education, 147, 28–40, https://doi.org/10.1111/j.1936-704x.2012.03105.x, 2012.

420 Giuntoli, I., Renard, B., Vidal, J. P., and Bard, A.: Low flows in France and their relationship to large-scale climate indices, Journal of Hydrology, 482, 105–118, https://doi.org/10.1016/j.jhydrol.2012.12.038, 2013.

Granger, C. W. J.: Investigating Causal Relations by Econometric Models and Cross-spectral Methods, Econometrica, 37, 424–438, http://ir.obihiro.ac.jp/dspace/handle/10322/3933, 1969.

Grinsted, A., Moore, J. C., and Jevrejeva, S.: Nonlinear Processes in Geophysics Application of the cross wavelet transform and wavelet coherence to geophysical time series, Nonlinear Processes in Geophysics, 11, 561–566, 2004.

Gudmundsson, L., Tallaksen, L. M., and Stahl, K.: Spatial cross-correlation patterns of European low, mean and high flows, Hydrological Processes, 25, 1034–1045, https://doi.org/10.1002/hyp.7807, 2011.

Hannaford, J., Lloyd-Hughes, B., Prudhomme, C., Parry, S., Keef, C., and Rees, G.: The Spatial Coherence of European Droughts – Final Report protecting and improving the environment in England and Wales, Tech. rep., Environment Agency's Science Programme., 2009.

430 Hubert, P.: Les multifractals, un outil pour surmonter les problèmes d'échelle en hydrologie, Hydrological Sciences Journal, 46, 897–905, https://doi.org/10.1080/02626660109492884, 2001.

Hubert, P., Carbonnel, J. P., and Chaouche, A.: Segmentation Des Séries Hydrométéorologiques - Application à des Séries de Précipitations et de Débits de L'Afrique de l'Ouest, Journal of Hydrology, 110, 349–367, https://doi.org/10.1016/0022-1694(89)90197-2, 1989.

IPCC: Climate Change 2007: The Physical Science Basis, Cambridge university press, https://doi.org/10.1017/CBO9781107415324.004, 435 2007.

IPCC: Climate change 2014. Synthesis report., Cambridge university press, https://doi.org/10.1017/CBO9781107415324, 2014.

Jajcay, N., Hlinka, J., Kravtsov, S., Tsonis, A. A., and Paluš, M.: Time scales of the European surface air temperature variability : The role of the 7 – 8 year cycle, Geophysical Research Letters, 43, 1–8, https://doi.org/10.1002/2015GL067325.Abstract, 2016.

Jajcay, N., Paluš, M., Kravtsov, S., Sugihara, G., Tsonis, A. A., Kravtsov, S., et al.: Synchronization and causality across time scales in El 440 Niño Southern Oscillation, npj Climate and Atmospheric Science, 1, 33, https://doi.org/10.1038/s41612-018-0043-7, 2018.

Joly, D., Brossard, T., Cardot, H., Cavailhes, J., Hilal, M., and Wavresky, P.: Les types de climats en France , une construction spatiale, Cybergeo : European Journal of Geography, p. 501, https://doi.org/10.4000/cybergeo.23155, 2010.

Kaufman, L. and Rousseeuw, P. J.: Finding Groups in Data: An Introduction to Cluster Analysis, Wiley interscience, https://doi.org/10.1007/s13398-014-0173-7.2, 1990.

445 Labat, D.: Non-Linéarité et Non-Stationnarité en Hydrologie Karstique, Ph.D. thesis, INP Toulouse, 2000.

Labat, D.: Oscillations in land surface hydrological cycle, Earth and Planetary Science Letters, 242, 143–154, https://doi.org/10.1016/j.epsl.2005.11.057, 2006.

Lambert, F. H., Webb, M. J., and Joshi, M. M.: The relationship between land-ocean surface temperature contrast and radiative forcing, Journal of Climate, 24, 3239–3256, https://doi.org/10.1175/2011JCLI3893.1, 2011.

450 Lavers, D., Prudhomme, C., and Hannah, D. M.: Large-scale climate, precipitation and British river flows: Identifying hydroclimatological connections and dynamics, Journal of Hydrology, 395, 242–255, https://doi.org/10.1016/j.jhydrol.2010.10.036, 2010.

Levine, P. A.: Land-atmosphere feedbacks in the energy, water, and carbon cycles of Earth system models, Ph.D. thesis, University of California, 2019.

Levine, P. A., Randerson, J. T., Swenson, S. C., and Lawrence, D. M.: Evaluating the strength of the land-atmosphere moisture 455 feedback in earth system models using satellite observation, Hydrology and Earth System Sciences Discussions, 20, 4837–4856, https://doi.org/10.5194/hess-2016-206, 2016.

Liu, D. and Graham, J.: Simple Measures of Individual Cluster-Membership Certainty for Hard Partitional Clustering, American Statistician, 73:1, 70–79, https://doi.org/10.1080/00031305.2018.1459315, 2018.

Lorenz, R., Argüeso, D., Donat, M. G., Pitman, A. J., Hurk, B. V. D., Berg, A., et al.: Influence of land-atmosphere feedbacks 460 on temperature and precipitation extremes in the GLACE-CMIP5 ensemble, Journal of Geophysical Research, 121, 607–623, https://doi.org/10.1002/2015JD024053, 2016.

Mariotti, A., Ruti, P. M., and Rixen, M.: Progress in subseasonal to seasonal prediction through a joint weather and climate community effort, npj Climate and Atmospheric Science, 1, 2–5, https://doi.org/10.1038/s41612-018-0014-z, 2018.

Massei, N., Durand, A., Deloffre, J., Dupont, J. P., Valdes, D., and Laignel, B.: Investigating possible links between the North Atlantic 465 Oscillation and rainfall variability in Northwestern France over the past 35 years, Journal of Geophysical Research Atmospheres, 112, 1–10, https://doi.org/10.1029/2005JD007000, 2007.

Massei, N., Dieppois, B., Hannah, D. M., Lavers, D. A., Fossa, M., Laignel, B., et al.: Multi-time-scale hydroclimate dynamics of a regional watershed and links to large-scale atmospheric circulation: Application to the Seine river catchment, France, Journal of Hydrology, 546, 262–275, https://doi.org/10.1016/j.jhydrol.2017.01.008, 2017.

470 McGregor, G.: Hydroclimatology, modes of climatic variability and stream flow, lake and groundwater level variability: A progress report, Progress in Physical Geography, 41, 496–512, https://doi.org/10.1177/0309133317726537, 2017.

Monti, S., Tamayo, P., Mesirov, J., and Golub, T.: Consensus clustering: A resampling-based method for class discovery and visualization of gene expression microarray data, Machine Learning, 52, 91–118, https://doi.org/10.1023/A:1023949509487, 2003.

Moron, V., Robertson, A. W., Ward, M. N., and Camberlin, P.: Spatial coherence of tropical rainfall at the regional scale, Journal of Climate, 475 20, 5244–5263, https://doi.org/10.1175/2007JCLI1623.1, 2007.

Nandi, B., Swiatek, P., Kocsis, B., and Ding, M.: Inferring the direction of rhythmic neural transmission via inter-regional phase-amplitude coupling (ir-PAC), Nature Scientific Reports, 9, 1–13, https://doi.org/10.1038/s41598-019-43272-w, 2019.

Onslow, A. C. E., Jones, M. W., and Bogacz, R.: A canonical circuit for generating phase-amplitude coupling, PLoS ONE, 9, https://doi.org/10.1371/journal.pone.0102591, 2014.

480 Paluš, M.: Cross-scale interactions and information transfer, Entropy, 16, 5263–5289, https://doi.org/10.3390/e16105263, 2014.

Palus, M.: Multiscale atmospheric dynamics: Cross-frequency phase-amplitude coupling in the air temperature, Physical Review Letters, 112, https://doi.org/10.1103/PhysRevLett.112.078702, 2014.

Pella, H., Lejot, J., Lamouroux, N., and Snelder, T.: The theoretical hydrographical network (RHT) for France and its environmental attributes, Geomorphologie: Relief, Processus, Environnement, 18, 317–336, https://doi.org/10.4000/geomorphologie.9933, 2012.

485   Pikovsky, A., Rosenblum, M., and Kurths, J.: Synchronization. A Universal Concept in Nonlinear Sciences, Cambridge University Press: Cambridge, 2001.

Rahiz, M. and New, M.: Spatial coherence of meteorological droughts in the UK since 1914, Area, 44, 400–410, https://doi.org/10.1111/j.1475-4762.2012.01131.x, 2012.

Sauquet, E., Gottschalk, L., and Krasovskaia, I.: Estimating mean monthly runoff at ungauged locations: an application to France, Hydrology
490   Research, 39, 403–423, https://doi.org/10.2166/nh, 2008.

Schaefli, B., Maraun, D., and Holschneider, M.: What drives high flow events in the Swiss Alps? Recent developments in wavelet spectral analysis and their application to hydrology, Advances in Water Resources, 30, 2511–2525, https://doi.org/10.1016/j.advwatres.2007.06.004, 2007.

Scheffer-Teixeira, R. and Tort, A. B. L.: On cross-frequency phase-phase coupling between theta and gamma oscillations in the hippocampus,
495   eLife, 5, 1–24, https://doi.org/10.7554/eLife.20515, 2016.

Scherrer, S.: Interannual climate variability in the European and Alpine region, Ph.D. thesis, ETH Zürich, https://doi.org/10.3929/ethz-a-005133273, 2006.

Schuite, J., Flipo, N., Massei, N., Rivière, A., and Baratelli, F.: Improving the Spectral Analysis of Hydrological Signals to Efficiently Constrain Watershed Properties, Water Resources Research, 55, 4043–4065, https://doi.org/10.1029/2018WR024579, 2019.

500   Sejas, S. A., Albert, O. S., Cai, M., and Deng, Y.: Feedback attribution of the land-sea warming contrast in a global warming simulation of the NCAR CCSM4, Environmental Research Letters, 9, https://doi.org/10.1088/1748-9326/9/12/124005, 2014.

Sidibe, M., Dieppois, B., Eden, J., Mahé, G., Paturel, J. E., Amoussou, E., et al.: Interannual to Multi-decadal streamflow variability in West and Central Africa: Interactions with catchment properties and large-scale climate variability, Global and Planetary Change, 177, 141–156, https://doi.org/10.1016/j.gloplacha.2019.04.003, 2019.

505   Smith, L., Turcotte, D., and Isacks, B.: Stream flow characterization and feature detection using a discrete wavelet transform, Hydrological processes, 12, 233–249, https://doi.org/10.1002/(SICI)1099-1085(199802)12:2<233::AID-HYP573>3.0.CO;2-3, 1998.

Snelder, T. H., Lamouroux, N., Leathwick, J. R., Pella, H., Sauquet, E., and Shankar, U.: Predictive mapping of the natural flow regimes of France, Journal of Hydrology, 373, 57–67, https://doi.org/10.1016/j.jhydrol.2009.04.011, 2009.

Sodemann, H. and Zubler, E.: Seasonal and inter-annual variability of the moisture sources for alpine precipitation during 1995-2002,
510   International Journal of Climatology, 30, 947–961, https://doi.org/10.1002/joc.1932, 2010.

Torrence, C. and Compo, G.: A Practical Guide to Wavelet Analysis., Bulletin of the American Meteorological Society, 79, 61–78, https://doi.org/10.1175/1520-0477(1998)079<0061:APGTWA>2.0.CO;2, 1998.

Vidal, J. P., Martin, E., Franchistéguy, L., Baillon, M., and Soubeyroux, J. M.: A 50-year high-resolution atmospheric reanalysis over France with the Safran system, International Journal of Climatology, 30, 1627–1644, https://doi.org/10.1002/joc.2003, 2010.

515   Wang, C., Osiński, M., Even, J., and Grillot, F.: Phase-amplitude coupling characteristics in directly modulated quantum dot lasers, Applied Physics Letters, 105, pp.233 103–2105, https://doi.org/10.1063/1.4903493, 2014.

Wang, L., Zhang, Y., and Feng, J.: On the Euclidean distance of images, IEEE Transactions on Pattern Analysis and Machine Intelligence, 27, 1334–1339, https://doi.org/10.1109/TPAMI.2005.165, 2005.

Şenbabaoğlu, Y., Michailidis, G., and Li, J. Z.: Critical limitations of consensus clustering in class discovery, Scientific Reports, 4, 6207,
520   https://doi.org/10.1038/srep06207, 2014.

Author contributions. conceptualization, Fossa M, Massei N and Dieppois B; methodology, Fossa M.; software, Fossa M; validation, Fossa M, Dieppois B, Massei N and Fournier M; formal analysis, Fossa M.; investigation, Fossa M; resources, Vidal JP.; data curation, Fossa M and Vidal JP; writing–original draft preparation, Fossa M; writing–review and editing, Fossa M, Dieppois B, Massei N and JP Vidal.; visualization, Fossa M

525 *Competing interests.* This reasearch work is part of a contribution to the EURO-Friend group 2.

Acknowledgements. The authors would like to thank Nikola Jajcay for his support with the adaptation of the Conditional Mutual Information algorithm (PyClits) to our context. The source code is available at https://github.com/jajcayn. The authors would also like to thank the Centre Régional Informatique et d'Applications Numériques de Normandie (CRIANN), for providing the HPC environment needed for all computations.